ACS Catalysis

Research Article

pubs.acs.org/acscatalysis

Highly Dispersed Ru on Electride $[Ca_{24}Al_{28}O_{64}]^{4+}(e^-)_4$ as a Catalyst for Ammonia Synthesis

Yasunori Inoue,[†] Masaaki Kitano,[‡] Sung-Wng Kim,[§,∥] Toshiharu Yokoyama,[§] Michikazu Hara,*[,†] and Hideo Hosono*[,†,‡,§]

[†]Materials and Structures Laboratory, Tokyo Institute of Technology, 4259 Nagatsuta, Midori-ku, Yokohama 226-8503, Japan

[‡]Materials Research Center for Element Strategy, Tokyo Institute of Technology, 4259 Nagatsuta, Midori-ku, Yokohama 226-8503, Japan

[§]Frontier Research Center, Tokyo Institute of Technology, 4259 Nagatsuta, Midori-ku, Yokohama 226-8503, Japan

Supporting Information

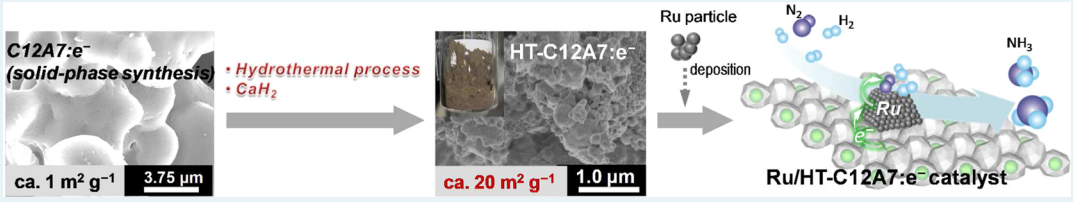

ABSTRACT: A high surface area $12CaO{\cdot}7Al_2O_3$ electride (HT-C12A7:e$^-$) was synthesized by the hydrothermal process and subsequent reduction with CaH_2 as a reducing agent, and was then examined as a support for a Ru catalyst in ammonia synthesis. Electrons are successfully incorporated into the cages of C12A7 powder by reduction with CaH_2 at 973 K. The concentration of encaged electrons increases with the dehydration temperature of the sample before the CaH_2 treatment. The surface area of the resulting material (ca. 20 $m^2\ g^{-1}$) is higher than that of the C12A7 electride prepared by conventional solid-phase reaction (SP-C12A7:e$^-$, ca. 1 $m^2\ g^{-1}$). The rate of ammonia synthesis over Ru/HT-C12A7:e$^-$ is twice that of Ru/SP-C12A7:e$^-$, and there is no significant difference in the apparent activation energy between both catalysts under the optimal conditions. Transmission electron microscopy (TEM) and CO chemisorption measurements revealed that Ru nanoparticles are more highly dispersed on HT-C12A7:e$^-$ than that on SP-C12A7:e$^-$, which results in the enhancement observed for ammonia synthesis.

KEYWORDS: *$[Ca_{24}Al_{28}O_{64}]^{4+}(e^-)_4$, ammonia synthesis, Ru, CaH_2, high surface area*

INTRODUCTION

Electrides[1,2] are crystals in which electrons serve as anions. Organic electrides have been conventionally prepared using alkali metal adducts of organic complexants, such as crown ethers and cryptants, but these electrides are thermally and chemically unstable. In 2003, an inorganic electride $[Ca_{24}Al_{28}O_{64}]^{4+}(e^-)_4$ (C12A7:e$^-$) was synthesized by utilizing a stable refractory oxide $12CaO{\cdot}7Al_2O_3$ (C12A7) which is a constituent of commercial alumina cement and acts as a complexant to electrons, instead of organic cyclic ethers, and the resulting material became the first electride that is stable in air above room temperature.[3] C12A7 is a mixed oxide of Ca and Al with a molar ratio of 12:14, and the chemical formula of a unit cell is expressed as $[Ca_{24}Al_{28}O_{64}]^{4+}(O^{2-})_2$. The former cation part is a positively charged lattice framework that possesses 12 sub-nanometer-size cages with an inner free space of ca. 0.4 nm in diameter. The latter anion part is comprised of free oxygen ions that are randomly trapped in 2 of the 12 cages to compensate the positive charge of the cage wall. The O^{2-} ions can be replaced by other anions, such as halogen anions (F^-, Cl^-),[4,5] hydroxide ions (OH^-),[6−10] superoxide radicals (O_2^-),[11,12] oxygen anion radicals (O^-),[11,12] sulfur ions (S^{2-}),[13] and hydride ions (H^-),[14−17] via appropriate treatment. In addition, severe reduction of C12A7 causes deficiency in the extraframework anions, which results in injection of electrons in the cages.[3] Therefore, the replacement of two free O^{2-} ions by four electrons leads to the formation of $[Ca_{24}Al_{28}O_{64}]^{4+}(e^-)_4$, which is abbreviated as C12A7:e$^-$. Hereafter, the injected electrons occupy a unique conduction band referred to as the "cage conduction band (CCB)", which is derived from the three-dimensionally connected cages.[18,19] The CCB has a relatively large dispersion. Thus, C12A7:e$^-$ exhibits metallic characteristics (1500 S cm^{-1}) at room temperature. Another unique property of C12A7:e$^-$ is a low work function of 2.4 eV. This value is comparable to that of metal potassium, but C12A7:e$^-$ is chemically inert contrary to the latter. Such a unique nature originates from the CCB and crystal structure; the Madelung potential is smaller than that of CaO due to the large separation between the cage center and the cage wall. Thus, the CCB position is pushed up to reduce the work function.[20]

Received: November 10, 2013
Revised: January 9, 2014
Published: January 15, 2014

Over the last several years, thin film, single crystal, and glass C12A7:e^- have been prepared by various chemical and physical methods. For example, C12A7 containing O^{2-} ions in the cages are reduced by Ti or Ca metal vapor and reducing gas such as CO/CO_2.[21,22] In addition to these chemical processes, a novel physical process of Ar^+ ion implantation in C12A7 films has been developed. However, these materials are unsuitable for catalysts because the surface areas of these materials are too small. It was found that powder-form C12A7 electride can be synthesized by a conventional solid-phase reaction.[23] Although the surface area of such C12A7 electride powder is only 1 m^2 g^{-1}, Ru-loaded C12A7 electride powder functions as an efficient catalyst for ammonia synthesis.[24] The Ru-loaded C12A7:e^- catalyst exhibits much higher catalytic activity than conventional Ru catalysts, which is attributed to strong electron-donating ability and reversible hydrogen-storage ability. C12A7:e^- powder is prepared by the solid-phase reaction of $CaCO_3$ with Al_2O_3 at 1573 K, followed by reduction at >1173 K.[23] This method results in a low surface area of the C12A7:e^-, at most only ca. 1 m^2 g^{-1}, which limits the catalytic performance of C12A7:e^-. The surface of the C12A7:e^- is completely covered with Ru nanoparticles, even with 0.3 wt % Ru loading (Ru dispersion of 5%).[24] C12A7:e^- with high surface area would increase the Ru dispersion and enhance the catalytic performance of Ru-loaded C12A7:e^- for ammonia synthesis. While various processes for the synthesis of C12A7 electride have been developed,[22] material with a high surface area has not yet been successfully synthesized. Li et al. reported that C12A7 with higher surface area (20−70 m^2 g^{-1}) than that for the conventional solid-phase reaction can be prepared by the hydrothermal reaction of $Al(OH)_3$ with $Ca(OH)_2$, followed by calcination at lower temperatures.[25] This material has no electrons in the cages, but this approach has potential for the synthesis of high surface area C12A7:e^-.

In the present study, C12A7:e^- with high surface area was successfully prepared for the first time by the calcination of hydrothermally produced Ca−Al mixed hydroxide, followed by reduction with CaH_2, which is a unique reducing agent that is used to reduce metal oxides at low temperatures.[26] In addition, the resultant material was examined as a support for Ru catalysts with an aim to enhance ammonia synthesis.

EXPERIMENTAL SECTION

Synthesis. High surface area C12A7:e^- powder was synthesized by the calcination of hydrothermally produced Ca−Al mixed hydroxide, followed by reduction with CaH_2. A stoichiometric mixture (Ca:Al = 12:14) of $Ca(OH)_2$ (>99%, Kojundo Chemical Lab. Co.) and $Al(OH)_3$ (99.99%, Kojundo Chemical Lab. Co.) was ball-milled in distilled water (160 mL) using a zirconia pot and yttria-stabilized zirconia balls (3 mm diameter) at a speed of 300 rpm. After 4 h, the mixture was heated in a Teflon-lined stainless autoclave (100 mL volume) at 423 K for 6 h with stirring. The product was separated by centrifugation at 3000 rpm and dried at 363 K overnight. The resultant Ca−Al mixed hydroxide material ($Ca_3Al_2(OH)_{12}$) was calcined at 873 K for 5 h in air, which resulted in the formation of C12A7 powder with a mayenite structure. The C12A7 powder prepared by the hydrothermal method is denoted as HT-C12A7. HT-C12A7 powder was heated at 873−1273 K (10 K min^{-1}) for 5 h in a vacuum (ca. 1×10^{-4} Pa) to remove water and hydroxyl groups incorporated in the cages and/or adsorbed on the surface. The evacuated HT-C12A7 powder (3 g) was mixed with an excess amount of CaH_2 (98%, Kanto Chemical Co., 0.4 g) in an Ar atmosphere. The mixture was sealed in a Ta tube within a silica tube under a vacuum, and was heated at 873−973 K (10 K min^{-1}) for 15 h (ca. 1×10^{-4} Pa). The resultant sample is denoted as HT-C12A7:e^-. For comparison, C12A7 electride powder (denoted as SP-C12A7:e^-) was also prepared by solid-phase reaction according to the procedure described in the literature.[23,24]

Catalyst Preparation. In accordance with the previous report,[24] 2 wt % Ru-loaded samples were prepared. HT-C12A7:e^- powder and $Ru_3(CO)_{12}$ (Aldrich Co.) were typically sealed in an evacuated silica tube and heated under the following temperature program: 2 K min^{-1} up to 313 K, hold for 1 h; 0.25 K min^{-1} up to 343 K, hold for 1 h; 0.4 K min^{-1} up to 393 K, hold for 1 h; 0.9 K min^{-1} up to 523 K, hold for 2 h; cool to ambient temperature.

Characterization of Catalyst. X-ray powder diffraction (XRD; Ultima-IV, Rigaku) and diffuse reflectance spectroscopy (DRS; V-670, Jasco) were used to characterize the structure of HT-C12A7:e^-. Phase transformation and crystallization temperatures of the HT-C12A7 powder were estimated from differential thermal analysis (DTA) and thermogravimetric (TG) measurements using a differential thermal analyzer (TG8120, Rigaku). The thermal desorption behavior of the sample was examined using temperature-programmed desorption-mass spectrometry (TPD-MS; TDS1200, ESCO). Nitrogen adsorption−desorption isotherms were measured at 77 K using a specific surface area analyzer (Nova 4200e, Quantachrome) after evacuation of the sample at 573 K. Ru dispersion was determined by the CO-pulse chemisorption method using an automatic gas-adsorption apparatus (BEL-CAT-A, BEL, Japan).[24] Prior to CO-pulse chemisorption, the samples were pretreated with a He flow (50 mL min^{-1}) at 673 K for 15 min, followed by a H_2 flow (50 mL min^{-1}) at 673 K for 15 min. Hydrogen atoms adsorbed on the reduced catalysts were removed by purging with He (50 mL min^{-1}) at 673 K for 15 min. To calculate the metal dispersion, a stoichiometry of Ru/CO = 1 was assumed.[27] Scanning electron microscopy (SEM; S-5200, Hitachi) and transmission electron microscopy (TEM; JEM-2010F, JEOL) were used to examine the morphology of the samples and the Ru particle size, respectively.

Activity Measurements. Ammonia reaction was performed under ambient pressure in the temperature range 593−673 K with a flow of stoichiometric H_2 and N_2 mixture (H_2/N_2 = 3, purity >99.99995%) gas at a rate of 60 mL min^{-1}, using a fixed-bed continuous-flow reactor containing 0.2 g of the catalyst. Prior to the reaction, the catalyst was reduced by flowing $N_2 + 3H_2$ gas mixture at 573 K for 5 h under ambient pressure. The ammonia produced was trapped in 5 mM H_2SO_4 aqueous solution, and the amount of NH_4^+ generated in the solution was determined using an ion chromatograph (LC-2000 plus, Jasco) equipped with a conductivity detector. To investigate the reproducibility, each catalyst was repeatedly tested at least three times. Average catalytic activities and error bars are shown in the results of the activity test.

RESULTS AND DISCUSSION

Structure of HT-C12A7e^-. Figure 1 shows powder XRD patterns of the as-prepared HT-C12A7 and HT-C12A7:e^-. The formation of single phase mayenite by the calcination of Ca−Al mixed hydroxide prepared by the hydrothermal method was confirmed, as shown by the XRD pattern for HT-C12A7. After calcination at 873 K, the surface area of HT-C12A7 was ca. 50

dx.doi.org/10.1021/cs401044a | ACS Catal. 2014, 4, 674−680

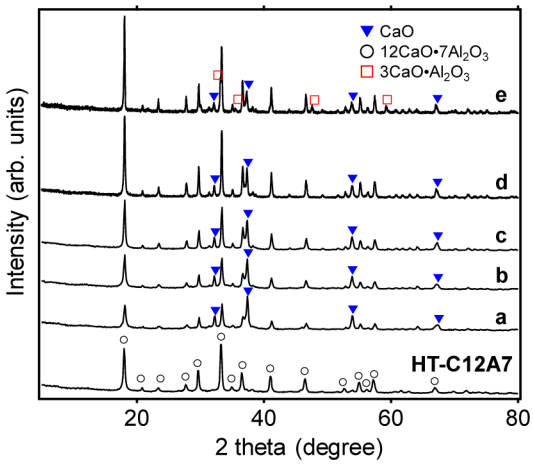

Figure 1. Powder XRD patterns for HT-C12A7 and HT-C12A7:e$^-$. HT-C12A7 was obtained after calcination of the Ca−Al mixed hydroxide at 873 K. HT-C12A7:e$^-$ was prepared by the reaction of HT-C12A7 and CaH_2 at 973 K. Before the reaction, HT-C12A7 was evacuated at (a) 873, (b) 973, (c) 1073, (d) 1173, and (e) 1273 K.

m^2 g^{-1}, which is much larger than that of C12A7 powder prepared by the conventional solid-phase reaction (ca. 1 m^2 g^{-1}). The HT-C12A7 powders were evacuated at various temperatures to remove water and then reduced with CaH_2 powder at 973 K to form HT-C12A7:e$^-$ powders. After the reduction reaction, mayenite and CaO phases were observed for all HT-C12A7:e$^-$ samples. CaO is produced from CaH_2 during the reduction. The intensity of the peaks for the mayenite phase increased with the temperature used for dehydration; however, the $3CaO{\cdot}Al_2O_3$ (C3A) phase was also observed at 1273 K, indicating that the framework structure of C12A7 is partially destroyed during dehydration at 1273 K. The average crystalline grain size, calculated from the (211) diffraction peak (2θ = 18.11°) using the Scherrer equation, was increased from ca. 25 to 55 nm with an increase in the dehydration temperature (see Table S1, Supporting Information). These values are somewhat smaller than that for SP-C12A7:e$^-$ (65 nm), which indicates that the preparation of C12A7:e$^-$ by the reduction of HT-C12A7 powder with CaH_2 is an effective method to prevent the aggregation of C12A7 particles, compared with that for the conventional solid-phase reaction. The Brunauer−Emmett−Teller (BET) surface areas measured for the HT-C12A7:e$^-$ samples are summarized in Table 1. The surface areas of HT-C12A7:e$^-$ are smaller than that of HT-C12A7 before reaction with CaH_2 and decrease

Table 1. BET Surface Area, Pore Volume, and Electron Density of the Obtained C12A7:e$^-$ Samples

sample	evacuation temperature[a] (K)	pore volume (cm^3 g^{-1})	S_{BET} (m^2 g^{-1})	electron density[b] (10^{21} cm^{-3})
HT-C12A7:e$^-$	873	0.155	46	
	973	0.105	37	
	1073	0.037	23	0.7
	1173	0.036	17	1.0
	1273	0.020	6	1.6
SP-C12A7:e$^-$ [c]	1273	0.002	1	2.0

[a]HT-C12A7 or C12A7 powder heated at these temperatures under 10^{-4} Pa. [b]Calculated from DRS results.[23] [c]Conventional C12A7:e$^-$ synthesized by solid-phase reaction.

with an increase in the dehydration temperature. The decrease in surface area is due to the aggregation of C12A7 nanoparticles, as shown in the SEM images of Figure 2.

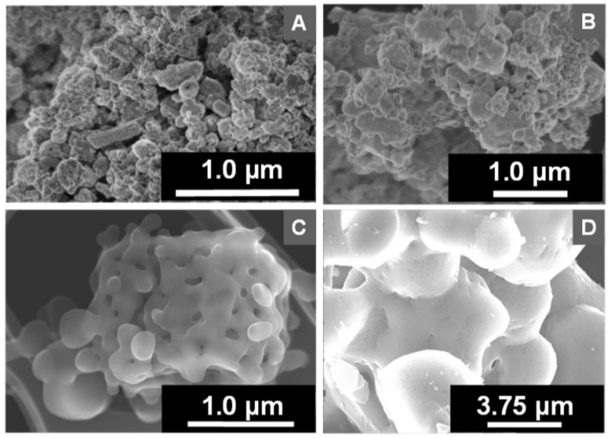

Figure 2. SEM images of HT-C12A7:e$^-$ prepared at various dehydration temperatures of (A) 1073, (B) 1173, and (C) 1273 K. (D) SP-C12A7:e$^-$ prepared by the conventional solid-phase reaction.

Although the average particle size of HT-C12A7:e$^-$ is increased from several hundred nanometers to more than 1 μm with an increase in the dehydration temperature, all the HT-C12A7:e$^-$ samples have larger surface areas than SP-C12A7:e$^-$ prepared by the solid-phase reaction.

Figure 3A shows the optical absorption spectra of HT-C12A7:e$^-$ prepared at various dehydration temperatures, in

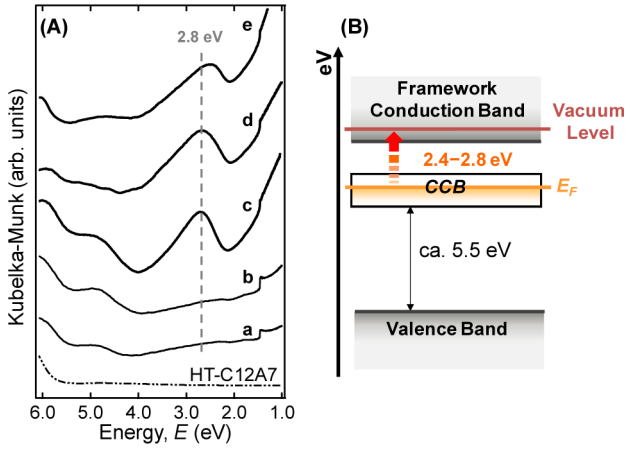

Figure 3. (A) Optical absorption spectra (obtained by Kubelka−Munk transformation of diffuse reflectance spectra) of HT-C12A7:e$^-$ samples prepared at various dehydration temperatures of (a) 873, (b) 973, (c) 1073, (d) 1173, and (e) 1273 K, and that of HT-C12A7 (dotted line). (B) Electronic structure of C12A7:e$^-$.[5]

addition to that for the as-prepared HT-C12A7 for comparison. The optical absorption edge of as-prepared HT-C12A7 was approximately 5.5 eV, which suggests that the absorption edge is dominated by absorption due to OH^- ions encaged in the framework cages.[5] It has been reported that extraframework OH^- ions are likely the most stable substitutive anions, because they easily replace extraframework O^{2-} ions when the C12A7 sample is treated in a wet atmosphere.[5] HT-C12A7 powder contains a large amount of OH^- ions in the framework cages, because it is prepared from a Ca−Al mixed hydroxide that

dx.doi.org/10.1021/cs401044a | ACS Catal. 2014, 4, 674−680

contains a large amount of water. After reduction with CaH_2, a broad absorption band was evident at around 2.8 eV, which is attributed to the intracage transition of electrons trapped in the cages.[22] Figure 3B shows that the trapped electrons occupy the unique CCB, which is derived from three-dimensionally connected cages formed by the sharing of one oxide monolayer.[22] This absorption band appears when HT-C12A7 powder is dehydrated at temperatures above 1073 K prior to treatment with CaH_2. Furthermore, the peak position is shifted to a lower energy side with the increase of the dehydration temperature up to 1273 K, which suggests that the concentration of trapped electrons in the cages increases with the dehydration temperature. Matsuishi et al. (ref 23) reported that the Fermi energy (E_F) varies with the increase in electron density (N_e) from 0.15 to 0.5 eV above the CCB minimum, and the absorption band position around 2−4 eV (E_{sp}) and electron density (N_e) are related to the following equation: $N_e = [-(E_{sp} - E_{sp}^{\circ})/0.199]^{0.782}$, where E_{sp}° = 2.83 eV at $N_e \approx 1 \times 10^{18}$ cm^{-3}. The electron concentrations of the HT-C12A7:e^- samples were estimated to be 0.7×10^{21}, 1.0×10^{21}, and 1.6×10^{21} cm^{-3}, according to the peak positions at 2.71, 2.64, and 2.47 eV, respectively (Table 1). Although these electron concentrations are lower than the theoretical maximum (2.33×10^{21} cm^{-3}), the C12A7 electride with high surface area (6−23 m^2 g^{-1}) has been successfully prepared by CaH_2 treatment of C12A7 powder derived from hydrothermally treated Ca−Al mixed hydroxide.

These results indicate that the electron concentration of HT-C12A7:e^- is largely dependent on the dehydration temperature. TG/DTA and TPD-MS measurements were conducted to elucidate the behavior of HT-C12A7 during dehydration. Figure 4A shows TG/DTA curves measured for HT-C12A7

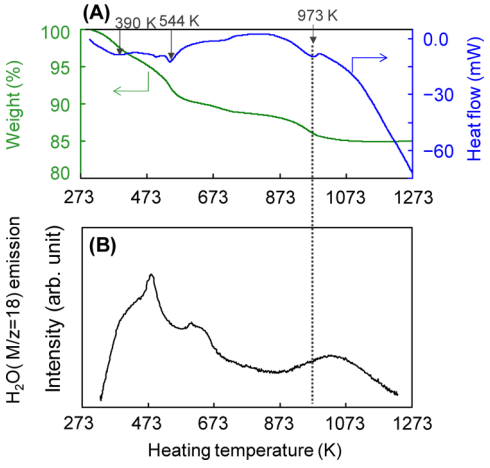

Figure 4. (A) TG/DTA profiles for HT-C12A7 powders in air (heating rate, 10 K min^{-1}). (B) TPD-MS spectrum for HT-C12A7 powders under a vacuum (heating rate, 30 K min^{-1}).

powder in air. A H_2O desorption (mass peak of m/z = 18) from the sample was evident in the TPD-MS spectrum shown in Figure 4B. The first weight loss and broad endothermic peaks observed in the range 300−600 K are attributed to the desorption of physisorbed water and the dehydration of hydroxyl groups in HT-C12A7 powder. Furthermore, additional weight loss and a H_2O emission peak were observed above 873 K, which is due to desorption of encaged OH^-.[7] This observation indicates that a H_2O molecule and O^{2-} ion are formed from two OH^- ions and the formed O^{2-} ions are then trapped in the cages ($2OH^- \rightarrow O^{2-} + H_2O$).[7] The absorption spectra shown in Figure S1A (Supporting Information) reveal a shift in the absorption band edge of HT-C12A7 to a lower energy side after dehydration. In addition, the intensity of the absorption band at around 5.0 eV increases with the dehydration temperature. It has been previously reported[5] that these absorption band edges around 5.7 and 4.6 eV can be attributed to extraframework OH^- and O^{2-} ions (Figure S1B, Supporting Information). Extraframework OH^- ions are therefore effectively replaced with O^{2-} ions by dehydration in the temperature range 973−1273 K, and the dehydrated HT-C12A7 powder easily reacts with CaH_2 to produce HT-C12A7:e^- according to the following reaction.

$$O^{2-} + CaH_2 \rightarrow 2e^- + CaO + H_2 \quad \text{(i)}$$

Thus, the dehydration process is essential for the synthesis of the C12A7 electride using CaH_2 as a reducing agent.

Activity of the Catalysts for Ammonia Synthesis. The catalytic performance of the Ru-loaded HT-C12A7:e^- (Ru/HT-C12A7:e^-) for the ammonia synthesis reaction was examined under atmospheric pressure. Figure 5 shows the

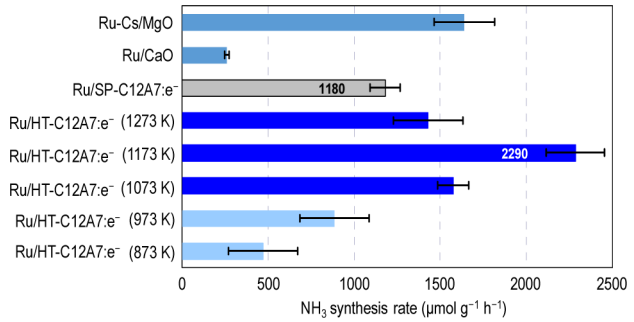

Figure 5. Reaction rate for ammonia synthesis over 2 wt % Ru-loaded HT-C12A7:e^- and various conventional Ru catalysts. The numbers in parentheses denote the dehydration temperatures. Reaction conditions: catalyst weight, 0.2 g; synthesis gas, H_2/N_2 = 3, 60 mL min^{-1}; pressure, 0.1 MPa; temperature, 613 K.

ammonia synthesis rate at 613 K for various 2 wt % Ru-loaded catalysts. The turnover frequency (TOF), apparent activation energy, mean Ru particle diameter, and Ru dispersion are summarized in Table 2. The NH_3 synthesis rate over Ru/HT-C12A7:e^- increases with increasing dehydration temperature and reaches a maximum for the sample dehydrated at 1173 K. However, the sample dehydrated at 1273 K has lower catalytic activity than that dehydrated at 1173 K. Under optimum conditions (dehydration at 1173 K), the NH_3 synthesis rate of Ru/HT-C12A7:e^- is twice that of Ru/SP-C12A:e^- and is superior to that of conventional Ru catalysts, such as Cs−Ru/MgO. The NH_3 thermodynamic limit under the reaction condition can be estimated to be about 7680 μmol g^{-1} h^{-1} (1.08 vol %). Therefore, the catalytic activity of Ru/HT-C12A7:e^- (1173 K) is about 30% that of the thermodynamic equilibrium.

The TEM image in Figure 6 indicates that the particle size of Ru on HT-C12A7:e^- is smaller than 10 nm, which is in good agreement with the results obtained by CO chemisorption (Table 2). The mean particle size of Ru on HT-C12A7:e^- is much smaller than that of Ru/SP-C12A7:e^-, despite having the same amount of Ru loading (2 wt %), which results in high Ru dispersion. The active site of the Ru catalyst for N_2 dissociation,

dx.doi.org/10.1021/cs401044a | ACS Catal. 2014, 4, 674−680

Table 2. Catalytic Performance of Ru Catalyst on Various Supports

catalyst	evacuation temperature (K)	dispersion (%)	particle size (nm)	TOF[a] (s^{-1})	E_a[b] (kJ mol^{-1})
Ru/HT-C12A7:e^-	873	38	4	0.0017	132
	973	51	3	0.0025	92
	1073	36	4	0.0069	75
	1173	14	9	0.0239	53
	1273	9	15	0.0225	63
Ru/SP-C12A7:e^-		3	42	0.0575	49
Cs-Ru/MgO[c]		19	7	0.0071	73

[a]TOFs were calculated from the rate of NH_3 synthesis divided by the number of CO atoms chemisorbed on the Ru surface. Reaction temperature: 613 K. [b]E_a is the apparent activation energy calculated from Arrhenius plots for the NH_3 synthesis rate in the temperature range 593−673 K. [c]Ru-loading: 6 wt %. The molar ratio was Ru:Cs = 1:1.

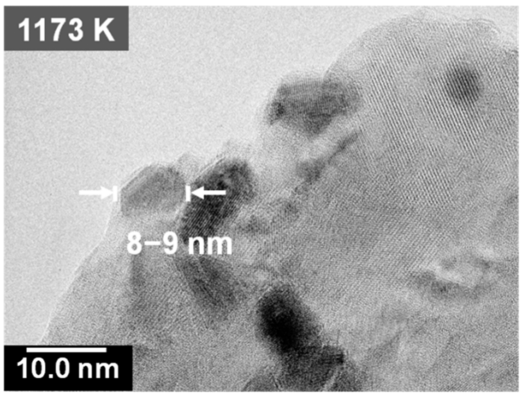

Figure 6. TEM image of Ru/HT-C12A7:e^- catalyst. HT-C12A7 was evacuated at 1173 K prior to reaction with CaH_2.

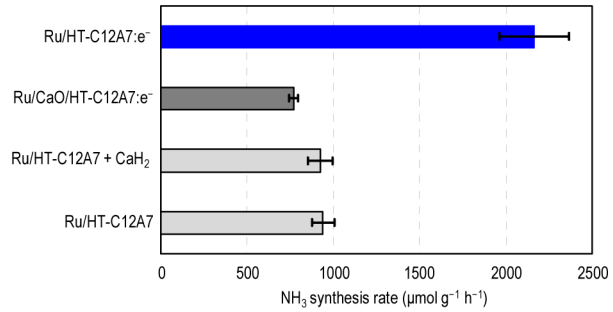

Figure 7. Reaction rate for ammonia synthesis over 2 wt % Ru-loaded HT-C12A7:e^- (1173 K) and various Ru-loaded HT-C12A7 catalysts. Reaction conditions: catalyst weight, 0.2 g; synthesis gas, H_2/N_2 = 3, 60 mL min^{-1}; pressure, 0.1 MPa; temperature, 613 K.

referred to as the B_5-type site, consists of Ru atoms; two at step edges and three at the lower terraces.[28,29] It has also been reported that the amount of B_5-type sites increases with a decrease in the particle size to reach a maximum at around 2.0 nm in diameter.[30] Therefore, the faster ammonia synthesis rate of Ru/HT-C12A7:e^- than Ru/SP-C12A7:e^- may be attributed to an increase in the number of B_5-type sites. Tables 1 and 2 show that the surface area and Ru dispersion of Ru/HT-C12A7:e^- prepared at 873 and 973 K are relatively higher than the other catalysts, although the NH_3 synthesis rate and TOF for these samples are inferior to that of Ru/SP-C12A7:e^-. In contrast, both the NH_3 synthesis rate and TOF for Ru/HT-C12A7:e^- prepared at >1073 K are larger than those prepared at <973 K, despite the low Ru dispersion and large Ru particle size. Therefore, the high catalytic performance of Ru/HT-C12A7:e^- prepared at >1073 K is not due to residual CaH_2 on the catalyst, because a Ru loaded mixture of CaH_2 and dehydrated HT-C12A7 exhibits much lower catalytic activity than the Ru/HT-C12A7:e^- catalyst and shows almost the same catalytic activity as Ru/HT-C12A7 (without electron). These results clearly indicate that CaH_2 has no promotional effect on the catalytic activity of Ru catalyst (Figure 7). Figure 3 shows that electrons are effectively introduced in the cages of HT-C12A7 when the dehydration temperature is higher than 1073 K. We have previously reported that high catalytic performance for NH_3 synthesis is achieved by efficient electron donation from C12A7:e^- to the antibonding orbital of N_2 through Ru nanoparticles.[24] Thus, the present results clearly indicate that electrons entrapped in the cages of HT-C12A7:e^- play a crucial role in NH_3 synthesis. Therefore, high catalytic performance cannot be obtained, even if small Ru nanoparticles are dispersed on HT-C12A7 without electrons in the cages. In addition, the apparent activation energy (E_a) of Ru/HT-C12A7:e^- decreases as the evacuation temperature is increased to 1173 K and reaches a minimum (53 kJ mol^{-1}) that is comparable to that for Ru/SP-C12A7:e^- (49 kJ mol^{-1}), as shown in Table 2. This result indicates that the electron donating efficiency of HT-C12A7:e^- (dehydration temperature: 1173 K) is comparable to that of Ru/SP-C12A7:e^-. The NH_3 synthesis rate over Ru/HT-C12A7:e^- dehydrated at 1273 K is inferior to that dehydrated at 1173 K, although the TOF values for both samples are comparable, because of the low surface area of Ru/HT-C12A7:e^- prepared at 1273 K.

It should be noted that the TOF values of Ru/HT-C12A7:e^- are less than half that of Ru/SP-C12A7:e^- (Table 2). One possible explanation for this phenomenon is the low crystallinity of HT-C12A7:e^-. According to the average crystallite size of each C12A7:e^- sample estimated from the (211) diffraction peak (Table S1, Supporting Information), Ru/HT-C12A7:e^- (1073 K) has a lower crystallinity than that dehydrated at 1173 K. The former electride catalyst does not have superior catalytic performance to the latter, despite having a high surface area and high electron concentration (Table 1). This suggests that the crystallinity of C12A7:e^- has a significant influence on NH_3 synthesis over Ru-loaded C12A7:e^-. Although the crystallite size of HT-C12A7:e^- increases with the dehydration temperature, HT-C12A7:e^- has a lower crystallinity than SP-C12A7:e^-. This idea could explain the lower TOF for HT-C12A7:e^-. Another possible explanation for the lower TOF of HT-C12A7:e^- is that CaO is formed during reduction with CaH_2 (Figure 1). The CaO phase would prevent not only the crystal growth of C12A7:e^-, but it would also decrease the amount of effective Ru particles on the

dx.doi.org/10.1021/cs401044a | ACS Catal. 2014, 4, 674−680

surface, because Ru particles on the CaO phase cannot function as effective sites for NH_3 synthesis. In addition, Figure 5 shows that the Ru/CaO catalyst has a much smaller catalytic performance than the other catalysts. To investigate the potential promotional role of CaO, we have prepared CaO-deposited HT-C12A7:e^- as a support for Ru catalyst. When 5.6 wt % Ca was deposited on the surface of HT-C12A7:e^- catalyst by heating a mixture of Ca metal and HT-C12A7 in a vacuum, CaO was observed on the surface of HT-C12A7:e^- (Figure S2, Supporting Information). The catalytic activity of Ru/CaO/HT-C12A7:e^- was much smaller than that of Ru/HT-C12A7:e^- (Figure 7), although both samples have the same electron concentration. This result clearly indicates that the surface CaO inhibits the electron donation from C12A7 electride to the surface Ru particles. From these results, intimate contact between Ru nanoparticles and HT-C12A7:e^- is indispensable for the efficient electron donation to Ru metal.

Figure 8 shows the correlation of the ammonia synthesis rate with the reaction time on stream. NH_3 is continuously

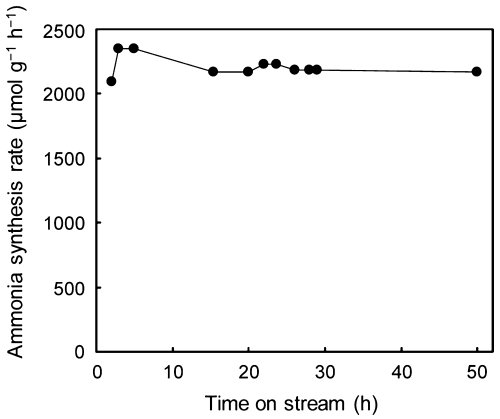

Figure 8. Time course of ammonia synthesis rate over Ru-loaded HT-C12A7:e^- at 613 K. HT-C12A7 was evacuated at 1173 K before the reaction with CaH_2. Reaction conditions: catalyst weight, 0.2 g; Ru loading, 2 wt %; synthesis gas, H_2/N_2 = 3, 60 mL min^{-1}; pressure, 0.1 MPa.

produced during 50 h without catalyst deactivation. When one electron is used for dissociation of one N_2 molecule, the NH_3 yield could be calculated to be 0.11 mmol (per catalyst weight; 0.2 g), which is 2 orders of magnitude lower than the total amount of ammonia production (22.6 mmol). Thus, HT-C12A7:e^- functions as a stable electronic promoter for ammonia synthesis reaction.

CONCLUSIONS

We successfully synthesized stable C12A7:e^- (HT-C12A7:e^-) with high surface area (ca. 20 m^2 g^{-1}) by the reduction of hydrothermally produced C12A7 powders with CaH_2. A high density of electrons (ca. 1.0×10^{21} cm^{-3}) can be introduced into the cages of HT-C12A7 powder by dehydration above 1073 K under a vacuum followed by reduction with CaH_2, because OH^- ions encaged in the HT-C12A7 powder are effectively replaced by O^{2-} ions above 1073 K. The NH_3 synthesis rate over the Ru/HT-C12A7:e^- catalyst was increased with the dehydration temperature and reached a maximum (2.4 mmol g^{-1} h^{-1}) at 1173 K, which is superior to that for conventional Ru catalysts (Ru/CaO, Ru−Cs/MgO), as well as that for Ru/SP-C12A7:e^-. The apparent activation energy for Ru/HT-C12A7:e^- with a high electron density and high surface area is very similar to that for Ru/SP-C12A7:e^-, which indicates that the electron-donating ability of HT-C12A7:e^- is sufficiently strong to promote N_2 dissociation on the Ru catalyst. The high catalytic performance of Ru/HT-C12A7:e^- is attributed to efficient electron donation from HT-C12A7:e^- to the highly dispersed Ru nanoparticles on the surface.

ASSOCIATED CONTENT

Supporting Information

Preparation of Ru catalyst on various supports, absorption spectra for as-prepared HT-C12A7, and HT-C12A7 evacuated at various dehydration temperatures, XRD pattern and SEM image of Ru supported on CaO/HT-C12A7:e^- powder evacuated at 1173 K, and crystallite diameter of various HT-C12A7:e^- samples. This material is available free of charge via the Internet at http://pubs.acs.org.

AUTHOR INFORMATION

Corresponding Authors

*E-mail: mhara@msl.titech.ac.jp.
*E-mail: hosono@msl.titech.ac.jp.

Present Address

[‖]Department of Energy Science, SungKyunKwan University, Suwon, Korea.

Notes

The authors declare no competing financial interest.

ACKNOWLEDGMENTS

This work was supported by a Funding Program for World-Leading Innovative R&D on Science and Technology from the Japan Society for the Promotion of Science and Japan Science and Technology Agency (JST) Accel program. We would like to express our sincere appreciation to Prof. Takashi Tatsumi and Assist. Prof. Toshiyuki Yokoi from Tokyo Institute of Technology for using the FE-SEM instrument and thank D. Lu (Material Analysis Suzukake-dai Center) for performing FE-TEM measurements. We would like to express our gratitude to Makoto Urano (ESCO Co.) and Naoyuki Sakamoto (MITSUBISHI CHEMICAL Co.) for their support. A very special thanks to Assoc. Prof. Katsuro Hayashi, Assist. Prof. Yoshitake Toda, and Kiyotaka Nakajima for beneficial discussions.

REFERENCES

(1) Dye, J. L. *Science* **1990**, *247*, 663−668.
(2) Dye, J. L. *Science* **2003**, *301*, 607−608.
(3) Matsuishi, S.; Toda, Y.; Miyakawa, M.; Hayashi, K.; Kamiya, T.; Hirano, M.; Tanaka, I.; Hosono, H. *Science* **2003**, *301*, 626−629.
(4) Jeevaratnam, J.; Glasser, F. P.; Glasser, L. S. D. *J. Am. Ceram. Soc.* **1964**, *47*, 105−106.
(5) Hayashi, K.; Sushko, P. V.; Ramo, D. M.; Shluger, A. L.; Watauchi, S.; Tanaka, I.; Matsuishi, S.; Hirano, M.; Hosono, H. *J. Phys. Chem. B* **2007**, *111*, 1946−1956.
(6) Imlach, J. A.; Dent Glasser, L. S.; Glasser, F. P. *Cem. Concr. Res.* **1971**, *1*, 57−61.
(7) Hayashi, K.; Hirano, M.; Hosono, H. *J. Phys. Chem. B* **2005**, *109*, 11900−11906.
(8) Nomura, T.; Hayashi, K.; Kubota, Y.; Kamiya, T.; Hirano, M.; Takata, M.; Hosono, H. *Chem. Lett.* **2007**, *36*, 902−903.
(9) Lee, D.-K.; Kogel, L.; Ebbinghaus, S. G.; Valov, I.; Wiemhoefer, H.-D.; Lerch, M.; Janek, J. *Phys. Chem. Chem. Phys.* **2009**, *11*, 3105−3114.

(10) Strandbakke, R.; Kongshaug, C.; Haugsrud, R.; Norby, T. *J. Phys. Chem. C* **2009**, *113*, 8938−8944.
(11) Hayashi, K.; Hirano, M.; Matsuishi, S.; Hosono, H. *J. Am. Chem. Soc.* **2002**, *124*, 738−739.
(12) Hayashi, K.; Matsuishi, S.; Ueda, N.; Hirano, M.; Hosono, H. *Chem. Mater.* **2003**, *15*, 1851−1854.
(13) Zhmoidin, G. I.; Chatterjee, A. K. *Cem. Concr. Res.* **1984**, *14*, 386−396.
(14) Hayashi, K.; Matsuishi, S.; Kamiya, T.; Hirano, M.; Hosono, H. *Nature* **2002**, *419*, 462−465.
(15) Bertoni, M. I.; Mason, T. O.; Medvedeva, J. E.; Freeman, A. J.; Poeppelmeier, K. R.; Delley, B. *J. Appl. Phys.* **2005**, *97*, 103713−103716.
(16) Matsuishi, S.; Hayashi, K.; Hirano, M.; Hosono, H. *J. Am. Chem. Soc.* **2005**, *127*, 12454−12455.
(17) Hayashi, K.; Sushko, P. V.; Shluger, A. L.; Hirano, M.; Hosono, H. *J. Phys. Chem. B* **2005**, *109*, 23836−23842.
(18) Li, Z.; Yang, J.; Hou, J. G.; Zhu, Q. *Angew. Chem., Int. Ed.* **2004**, *43*, 6479−6482.
(19) Sushko, P. V.; Shluger, A. L.; Hirano, M.; Hosono, H. *J. Am. Chem. Soc.* **2007**, *129*, 942−951.
(20) Toda, Y.; Yanagi, H.; Ikenaga, E.; Kim, J. J.; Kobata, M.; Ueda, S.; Kamiya, T.; Hirano, M.; Kobayashi, K.; Hosono, H. *Adv. Mater.* **2007**, *19*, 3564−3569.
(21) Kim, S.-W.; Matsuishi, S.; Nomura, T.; Kubota, Y.; Takata, M.; Hayashi, K.; Kamiya, T.; Hirano, M.; Hosono, H. *Nano Lett.* **2007**, *7*, 1138−1143.
(22) Kim, S.-W.; Matsuishi, S.; Miyakawa, M.; Hayashi, K.; Hirano, M.; Hosono, H. *J. Mater Sci.: Mater. Electron.* **2007**, *18*, 5−14.
(23) Matsuishi, S.; Nomura, T.; Hirano, M.; Kodama, K.; Shamoto, S.-i.; Hosono, H. *Chem. Mater.* **2009**, *21*, 2589−2591.
(24) Kitano, M.; Inoue, Y.; Yamazaki, Y.; Hayashi, F.; Kanbara, S.; Matsuishi, S.; Yokoyama, T.; Kim, S.-W.; Hara, M.; Hosono, H. *Nat. Chem.* **2012**, *4*, 934−940.
(25) Li, C.; Hirabayashi, D.; Suzuki, K. *Mater. Res. Bull.* **2011**, *46*, 1307−1310.
(26) Tsujimoto, Y.; Tassel, C.; Hayashi, N.; Watanabe, T.; Kageyama, H.; Yoshimura, K.; Takano, M.; Ceretti, M.; Ritter, C.; Paulus, W. *Nature* **2007**, *450*, 1062−1065.
(27) Larichev, Y. V.; Moroz, B. L.; Zaikovskii, V. I.; Yunusov, S. M.; Kalyuzhnaya, E. S.; Shur, V. B.; Bukhtiyarov, V. I. *J. Phys. Chem. C* **2007**, *111*, 9427−9436.
(28) Dahl, S.; Törnqvist, E.; Chorkendorff, I. *J. Catal.* **2000**, *192*, 381−390.
(29) Dahl, S.; Sehested, J.; Jacobsen, C. J. H.; Törnqvist, E.; Chorkendorff, I. *J. Catal.* **2000**, *192*, 391−399.
(30) Honkala, K.; Hellman, A.; Remediakis, I. N.; Logadottir, A.; Carlsson, A.; Dahl, S.; Christensen, C. H.; Nørskov, J. K. *Science* **2005**, *307*, 555−558.